Mechanistic Model for Spade Drills for Wood Drilling Operations, Part 1: Model Development

Hanxin Zhao

Kornel F. Ehmann

Department of Mechanical Engineering,
Northwestern University,
2145 Sheridan Road,
Evanston, IL 60208-3111

The purpose of this work is to present an investigation of the force system generated during spade drill-bit drilling processes that is a prerequisite for the design of spade-drills with improved performance. The technical literature offers no references to this type of bit and process; hence an approach based on the well-established mechanistic force prediction methods will be used. The force and torque prediction models are based on a complete analytical model of a generalized spade bit that takes into account the cutting action of all the characteristic cutting edges of the spade bit, namely of its chisel edge, tip and major cutting edges. In conjunction with the model an efficient model calibration method is also introduced and experimentally verified. [DOI: 10.1115/1.1559156]

1 Introduction

The spade drill bit is a very widely used tool in the construction industry for drilling in wood and wood based products for plumbing and electrical installations. The basic design of the tool has not changed for decades. The introduction of hand-held battery-operated cordless drills has, however, imposed the need to improve the performance of these tools in two respects: (1) reduced power consumption in order to prolong battery life, and (2) reduced thrust force to reduce operator fatigue. This, in turn, necessitates the examination of the suitability of the existing ubiquitous design and of the possibility of developing new bits with enhanced performance. In either case, to meet these goals in the most efficient way, a systematic approach, based on a sound theoretical foundation, is needed to guide the evaluation and design effort. Such an approach is in particular paramount since currently new developments are entirely based on ad-hoc trial and error procedures.

The review of the technical literature does not yield any publication related to this particular type of drill and drilling operation, hence both geometric and cutting mechanics aspects of this tool need to be developed before a systematic design process can be put in place. An attempt toward this objective was given by Zhao [1]. In a two-part publication Zhao et al. [2] develop the analytical foundation for the definition of the geometry and manufacture of these bits. It is objective of this paper to develop a basic model for the cutting mechanics aspects of spade drills. This model will be based on the aforementioned drill geometry model and will utilize the widely used mechanistic approach.

Upon complete definition of the mechanistic models all prerequisites will exist to assess the performance of a wood drilling spade bit, expressed in terms of machining forces and energy, drill bit wear, drill bit breakage and hole quality, as well as provide a basis and a set of design tools for new developments.

It is commonly known that many problems still exit in terms of the complete understanding of the drilling process, including those related to form errors, burrs, chatter, and tool wear and failure. Generally, the cutting forces that depend on tool geometry parameters and machining conditions contain information on the sources of these problems. Therefore, accurate mechanistic models are a necessity for estimating the components of the force system acting on the drill's cutting edges in order to find optimized designs for new tool geometries, to improve quality, and to increase productivity.

Mechanistic models have been used in the past to predict the force system in machining processes including end milling [3,4] and drilling [5–9]. The mechanistic approach is based on the geometry of the process and relates the cutting forces to the chip load through the specific forces, which are empirically determined from fundamental machining parameters. The model coefficients for a given tool and workpiece material combination are determined from calibration experiments. In the past, researchers have used calibration data from orthogonal or oblique cutting operations, or turning to predict the forces in other processes such as end milling [10,11] and drilling [12–14].

This paper will introduce an elemental mechanistic cutting model and the formulation of the procedure for computing the resultant forces acting on the major cutting edge, tip cutting edge and chisel edge of spade drills used in wood drilling operations. In conjunction with the model a generalized calibration algorithm will be introduced to determine the model coefficients from force data obtained from specially designed spade drilling experiments.

2 Mechanistic Force Model

Merchant [15] has shown, by using conservation of energy methods, that if the chip is held in equilibrium by the resultant machining forces, the cutting forces that act on the tool in the equivalent two-dimensional rake-face or machine-tool coordinate system are proportional to the uncut chip area or chip load. The chip load is the projected area of the shear plane measured in a plane normal to the cutting-velocity vector. The constant of proportionality, the specific cutting pressure, was later found to be dependent on the cutting conditions, tool geometry, the uncut chip thickness (t_c), the normal rake angle (γ_n) and cutting velocity (V).

Using this concept Gu et al. [16], Endres and Waldorf [17] and others have used the rake-face coordinate frame (shown in Fig. 1) and assumed that the magnitude of the force normal to the rake face of the tool, i.e., the Normal Force ($|F_n|$), and the force on the rake face in the direction of chip flow, i.e., the Friction Force ($|F_f|$), are both proportional to the chip area. The two rake-face forces and the chip flow direction fully characterize the force system on the cutting tool and are used to develop the drilling force model as well. The magnitudes of the normal and friction forces are given by the mechanistic equations:

Contributed by the Manufacturing Engineering Division for publication in the JOURNAL OF MANUFACTURING SCIENCE AND ENGINEERING. Manuscript received October 2001; Revised October 2002. Associate Editor: Yung Shin.

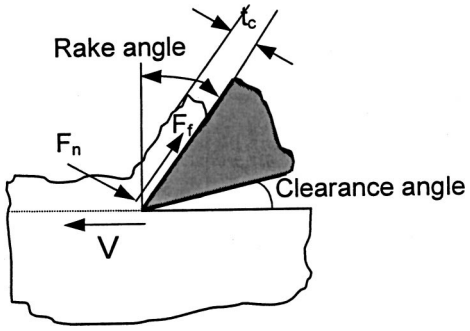

Fig. 1 Chip removal model

$$|F_n| = K_n A_c$$
$$|F_f| = K_f A_c \tag{1}$$

The chip area, A_c is defined in the plane whose normal is coincident with the direction of the cutting velocity. K_n and K_f are defined to be the Specific Normal Force and the Specific Friction Force.

It is well documented and accepted that the specific normal and friction forces depend on the chip thickness and velocity and are modeled by a power law. However, to date there is no standard way of including the rake angle effect. Some researchers (e.g., Endres and Waldorf, [17]) use the effective-rake angle while others (e.g., Chandreasekharan et al., [8,9]) include the normal-rake angle in the empirical model. While each argument presented has its merits, no conclusive data from actual experiments has been presented. Modeling the effect of the rake angle on the specific forces is a critical step in standardizing the force models as the rake angle can vary considerably across tool geometries and processes. Chandreasekharan et al. [8] have found that the average percentage variation for the resultant normal and friction forces is reasonably small considering that the effective-rake angle varies over a fairly wide range and there is no consistent trend or correlation between the force components and the effective-rake angle. Consequently, the following empirical equations can be used to compute the specific normal and friction forces in terms of the chip thickness (t_c), cutting velocity (V) and normal-rake angle (γ_n).

$$\begin{cases} \ln K_n = a_0 + a_1 \ln t_c + a_2 \ln V + a_3 \gamma_n \\ \ln K_f = b_0 + b_1 \ln t_c + b_2 \ln V + b_3 \gamma_n \end{cases} \tag{2}$$

For conventional drilling operations the influence of the clearance angle is negligible; hence it has generally been omitted from mechanistic models. From a comprehensive set of systematic preliminary experiments performed by commercially available and prototype spade drill bits it became evident that the influence of the clearance angle can become significant [1]. Therefore, in the current research expanded relationships will be introduced to express the influence of the clearance angle, α_n, on the specific normal and friction forces. This will be accomplished by adding an additional term into Eq. (2), i.e.:

$$\begin{cases} \ln K_n = a_0 + a_1 \ln t_c + a_2 \ln V + a_3 \gamma_n + a_4 \alpha_n \\ \ln K_f = b_0 + b_1 \ln t_c + b_2 \ln V + b_3 \gamma_n + b_4 \alpha_n \end{cases} \tag{3}$$

where a_i and b_i, $i = 1, 2, 3$ and 4 are coefficients that generally need to be determined from suitably collected experimental data. This process, referred to as model calibration, typically needs to be performed whenever the machining conditions undergo a significant change. Equation (3) will be used henceforth in the analyses and modeling of the force system acting on spade bits.

The above expressions express the forces in the rake-face coordinate frame and are general in nature. These expressions will be applied next to define the elemental forces in the general coordinate frame as the first step in building a complete mechanistic model for spade drilling operations.

2.1 Oblique-Cutting Based Elemental Force Model for Spade Bits. The generalized geometry of spade bits, defined in detail in [1,2], is shown in Fig. 2, which also identifies the principal cutting edges of this tool. In its most general form the rake surface is a helicoid defined by a straight or curved generator twisted by the helix angle δ, the intersection of which with a properly defined clearance/flank surface generator (e.g., grinding wheel) defines the major, tip and chisel edges. Frequently, to increase the rake angle distribution along an edge a micro-groove is added. Almost without exception the tip portion always has a micro-groove, while this feature, given different design realizations, is also frequently present along the major cutting edge. This is necessary since the overwhelming majority of commercially available drills use a planar rake surface ($\delta = 0$).

The spade drilling process is a true oblique-cutting process; hence a third force component—the lateral force—is also present. To develop accurate models for the force components that act on the cutting edges of a spade drill bit, a basic mechanistic force model for the oblique-cutting process must be established. The oblique-cutting elemental forces are then resolved in the drilling coordinate frame and summed to obtain the total forces.

To develop a three-dimensional mechanistic model for the spade drilling processes the cutting edges of the drill are divided into small elements [5] (Fig. 3). To determine the specific normal force and the specific friction force acting on each element, the chip thickness, cutting velocity, the normal rake angle and the normal clearance angle must be determined. The chip thickness (t_c) is defined to be the thickness normal to the cutting edge (Fig. 3). The analytical expressions for the variation of the cutting angles with the radial distance coordinate for different spade bit topologies have been derived in [1,2].

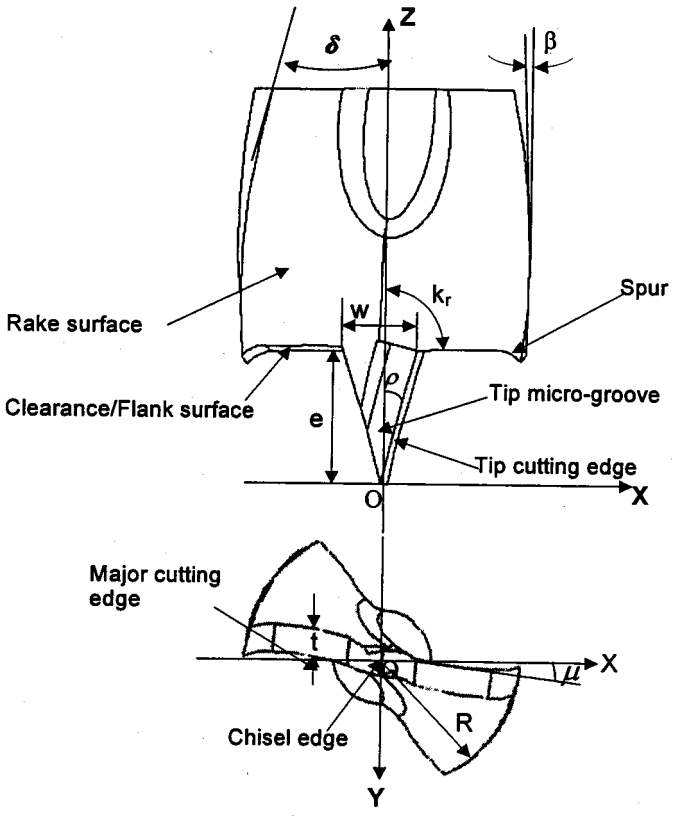

Fig. 2 Generalized helical spade bit geometry

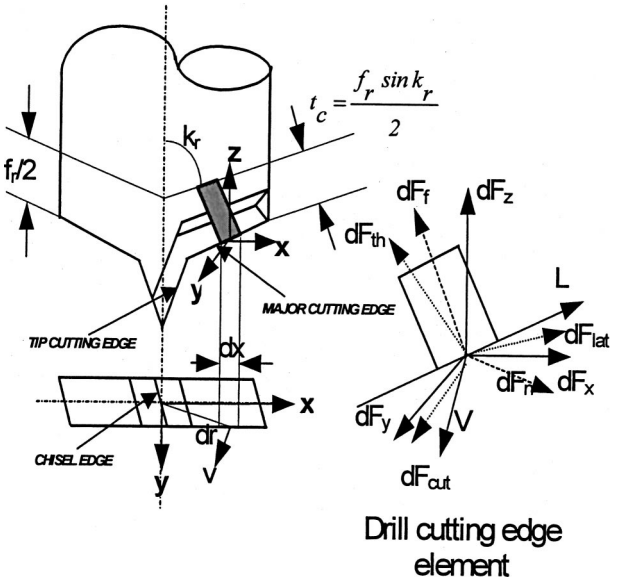

Fig. 3 Elemental model for the cutting edges of the spade drill bit

Due to the difference between the direction in which the forces are measured and the normal and friction force directions, three different coordinate frames need to be introduced. The first is the rake face coordinate frame ($dF_n dF_f dF_w$), which is defined by the direction of the elemental friction force dF_f, the elemental normal force dF_n and a direction perpendicular to the previous two to be designated by dF_w (no force component acts in this direction). In the rake-face coordinate frame, the magnitudes of the elemental normal force ($|dF_n|$) and of the friction force ($|dF_f|$) are computed from the mechanistic model Eq. (1). The elemental friction force dF_f acts on the rake face, along the chip flow direction, while the elemental normal force dF_n acts on the plane that is normal to the rake face and the main cutting edge. The direction dF_w is determined by the cross-product of dF_n and dF_f.

The second coordinate frame is the drilling coordinate frame, which is formed by the elemental oblique-cutting Thrust Force $|dF_{\text{th}}|$, Cutting Force $|dF_{\text{cut}}|$, and Lateral Force $|dF_{\text{lat}}|$. These three force components can be computed from the elemental normal and friction forces. The elemental cutting force $|dF_{\text{cut}}|$ acts in the direction of the cutting velocity vector. The direction of the elemental oblique-cutting thrust force $|dF_{\text{th}}|$ is defined by the cross product of unit vectors in the direction of the velocity and of the cutting edge element, i.e., $V \times L/|V \times L|$. Here, the origin of the coordinate system is placed at the mid-point of the drill-bit's cutting edge element (Fig. 3). The unit vector in the direction of the cutting edge element (L) and the velocity vector (V) are defined in this frame. The direction of the elemental lateral force $|dF_{\text{lat}}|$ is then given by $-dF_{\text{cut}} \times dF_{\text{th}}/|dF_{\text{cut}} \times dF_{\text{th}}|$.

The third coordinate frame is the general coordinate frame, which includes the elemental drilling thrust dF_z and radial forces dF_x and dF_y. The elemental drilling thrust dF_z and radial forces, dF_x and dF_y, are determined by vector decomposition.

The magnitude of the elemental drilling thrust force $|dF_z|$ and of the radial forces $|dF_x|$ and $|dF_y|$ are then just the x, y and z components of the resultant three-dimensional oblique-cutting force acting on each element. The elemental torque $|dM_z|$ is the product of the radial distance of the element and of the cutting force dF_{cut}.

The magnitude of the total drilling thrust $|F_z|$, torque $|M_z|$ and of the radial forces $|F_x|$ and $|F_y|$ for any portion of the cutting edges of the drill can be obtained by evaluating the elemental thrust force dF_z, elemental radial forces dF_x and dF_y from the rake face coordinate frame ($dF_n dF_f dF_w$) shown in Figure 3 and summing the corresponding thrust, torque and radial forces of all elements in that region for both cutting edges. In the sequel the relationships between elemental forces will be established.

2.2 The Relationships Between Elemental Force Components. Using the preceding definitions of the different force coordinate frames, the relationships between the measured forces and the elemental specific forces can be established. To transform the elemental normal and friction forces into the elemental thrust and torque, first of all the relationships between the rake-face coordinate system $dF_n dF_f dF_w$ and the drilling coordinate system $dF_{\text{th}} dF_{\text{lat}} dF_{\text{cut}}$, both shown in Fig. 4, needs to be defined.

Figure 4 presents an oblique cutting element with an inclination angle i. The rake-face coordinate system $dF_n dF_f dF_w$ corresponds to the effective cutting position. The drilling coordinate system $dF_{\text{th}} dF_{\text{lat}} dF_{\text{cut}}$ represents the elemental oblique-cutting position that has been defined above. The origin of these two coordinate systems, "o," is located at the center point of the cutting element. Plane "oce" represents the elemental rake face. According to ANSI B94.50-1975, the tool reference plane P_r is the plane "oars"; the tool cutting edge plane P_s is the plane "oss"; the cutting edge normal plane P_n is the plane "oac." Thus the angle $\gamma_n (\angle aoc)$ corresponds to the normal rake angle, $\eta_c (\angle coe)$ to the chip flow angle and i to the inclination angle. To transform entities from the $dF_{\text{th}} dF_{\text{lat}} dF_{\text{cut}}$ coordinate system into the $dF_n dF_f dF_w$ coordinate system, the following three steps need to be performed:

1) The frame $dF_{\text{th}} dF_{\text{lat}} dF_{\text{cut}}$ needs to be rotated by the angle i about the dF_{th} axis (Rot1(dF_{th},i)) with respect to the $dF_{\text{th}} dF_{\text{lat}} dF_{\text{cut}}$ frame:

$$\text{Rot1}(dF_{\text{th}}, i) = \begin{bmatrix} \cos i & -\sin i & 0 \\ \sin i & \cos i & 0 \\ 0 & 0 & 1 \end{bmatrix} \tag{4}$$

2) The frame $dF_{\text{th}} dF_{\text{lat}} dF_{\text{cut}}$ needs to be rotated by an angle 90-γ_n about the dF_{lat} axis (Rot2(dF_{lat},90-γ_n)) with respect to the $dF_{\text{th}} dF_{\text{lat}} dF_{\text{cut}}$ frame:

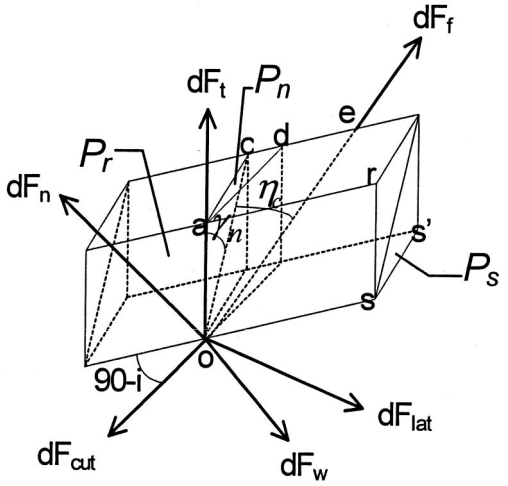

Fig. 4 Oblique elemental cutting forces (Frames $dF_{\text{th}} dF_{\text{lat}} dF_{\text{cut}}$ and $dF_n dF_f dF_w$)

$$\text{Rot2}(dF_{\text{lat}},90-\gamma_n)=\begin{bmatrix}1 & 0 & 0\\ 0 & \cos(90-\gamma_n) & -\sin(90-\gamma_n)\\ 0 & \sin(90-\gamma_n) & \cos(90-\gamma_n)\end{bmatrix}$$

$$=\begin{bmatrix}1 & 0 & 0\\ 0 & \sin\gamma_n & -\cos\gamma_n\\ 0 & \cos\gamma_n & \sin\gamma_n\end{bmatrix} \quad (5)$$

3) The frame $dF_{\text{th}}dF_{\text{lat}}dF_{\text{cut}}$ needs to be rotated by an angle η_c about the dF_{th} axis $(\text{Rot3}(dF_{\text{th}},\eta_c))$ with respect to the $dF_{\text{th}}dF_{\text{lat}}dF_{\text{cut}}$ frame:

$$\text{Rot3}(dF_{\text{th}},-\eta_c)=\begin{bmatrix}\cos(-\eta_c) & -\sin(-\eta_c) & 0\\ \sin(-\eta_c) & \cos(-\eta_c) & 0\\ 0 & 0 & 1\end{bmatrix} \quad (6)$$

Combining all three steps, yields:

$$\begin{bmatrix}dF_{\text{lat}}\\ dF_{\text{cut}}\\ dF_{\text{th}}\end{bmatrix}=\text{Rot1}(dF_{\text{th}},i).\text{Rot2}(dF_{\text{lat}},90-\gamma_n).\text{Rot3}(dF_{\text{th}},-\eta_c).\begin{bmatrix}dF_w\\ dF_f\\ -dF_n\end{bmatrix}$$

$$=\begin{bmatrix}-\cos\gamma_n\sin i dF_n+dF_f(\cos i\sin i-\cos i\sin i\sin\gamma_n)\\ dF_n\cos i\cos\gamma_n+dF_f(\sin^2 i+\cos^2 i\sin\gamma_n)\\ -dF_n\sin\gamma_n+dF_f\cos i\cos\gamma_n\end{bmatrix} \quad (7)$$

Since the chip always exerts a compressive force on the rake face, this leads to the normal cutting force $-dF_n$. Also one should note that the force component dF_w is always equal to zero by definition.

Now, by considering the transformation between the general coordinate system $dF_xdF_ydF_z$ and the drilling coordinate system $dF_{\text{th}}dF_{\text{lat}}dF_{\text{cut}}$, according to Fig. 5, the transformation between these two frames can be accomplished in two steps. The first step is to rotate the frame $dF_xdF_ydF_z$ by an angle $-i$ about the dF_z axis $(\text{Rot1}(dF_z,-i))$ with respect to the $dF_xdF_ydF_z$ frame:

$$\text{Rot1}(dF_z,-i)=\begin{bmatrix}\cos(-i) & -\sin(-i) & 0\\ \sin(-i) & \cos(-i) & 0\\ 0 & 0 & 1\end{bmatrix} \quad (8)$$

while the second step is to rotate the frame $dF_xdF_ydF_z$ by an angle $90-k_r$ about the dF_y axis $(\text{Rot2}(dF_y,90-k_r))$ with respect to the $dF_xdF_ydF_z$ frame:

$$\text{Rot2}(dF_y,90-k_r)=\begin{bmatrix}\cos(90-k_r) & 0 & -\sin(90-k_r)\\ 0 & 1 & 0\\ \sin(90-k_r) & 0 & \cos(90-k_r)\end{bmatrix}$$

$$=\begin{bmatrix}\sin k_r & 0 & -\cos k_r\\ 0 & 1 & 0\\ \cos k_r & 0 & \sin k_r\end{bmatrix} \quad (9)$$

Thus, based on the above, the relationship between the $dF_xdF_ydF_z$ and the $dF_{\text{th}}dF_{\text{lat}}dF_{\text{cut}}$ coordinate systems becomes:

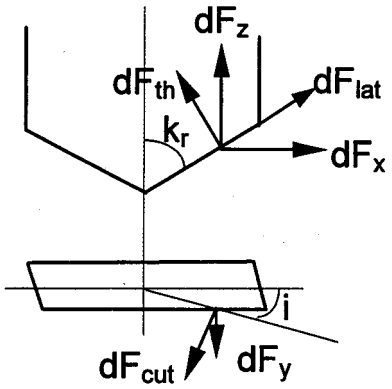

Fig. 5 The relation between frames $dF_{\text{th}}dF_{\text{lat}}dF_{\text{cut}}$ and $dF_xdF_ydF_z$

$$\begin{bmatrix}dF_x\\ dF_y\\ dF_z\end{bmatrix}=\text{rot1}(dF_z,-i).\text{Rot2}(dF_y,90-k_r)\begin{bmatrix}dF_{\text{lat}}\\ dF_{\text{cut}}\\ dF_{\text{th}}\end{bmatrix}$$

$$=\begin{bmatrix}dF_{\text{lat}}\cos i\sin k_r+dF_{\text{cut}}\sin i-dF_{\text{th}}\cos i\cos k_r\\ -dF_{\text{lat}}\sin i\sin k_r+dF_{\text{cut}}\cos i+dF_{\text{th}}\sin i\cos k_r\\ dF_{\text{lat}}\cos k_r+dF_{\text{th}}\sin k_r\end{bmatrix} \quad (10)$$

Here $dF_xdF_ydF_z$ defines the general coordinate system and dF_z also represents the general elemental thrust force. The elemental torque dM_z, according to the drilling system $dF_{\text{th}}dF_{\text{cut}}dF_{\text{lat}}$, is equal to:

$$|dM_z|=|r|.|dF_{\text{cut}}| \quad (11)$$

By substituting dF_{cut} from Eq. (7) into Eq. (11) an expression for the elemental torque in terms of the elemental normal force and the friction force is obtained as:

$$|dM_z|=|r|[|dF_f|(\sin^2 i+\cos^2 i\sin\gamma_n)+|dF_n|\cos i\cos\gamma_n] \quad (12)$$

Based on the above analysis, one easily obtains the relationship between the general coordinate force frame $dF_xdF_ydF_z$ and the rake face coordinate force frame $dF_ndF_fdF_w$ as given below:

$$\begin{bmatrix}dF_x\\ dF_y\\ dF_z\end{bmatrix}=\text{Rot1}(dF_z,-i).\text{Rot2}(dF_y,90-k_r).\text{Rot1}(dF_{\text{th}},i).\text{Rot2}(dF_{\text{lat}},90-\gamma_n).\text{Rot3}(dF_{\text{th}},-\eta_c).\begin{bmatrix}dF_w\\ dF_f\\ -dF_n\end{bmatrix} \quad (13)$$

Furthermore, according to Stabler's rule [18], assuming that $\eta_c=i$, and substituting $\text{Rot1}(dF_{\text{th}},i)$, $\text{Rot2}(dF_{\text{lat}},90-\gamma_n)$, $\text{Rot3}(dF_{\text{th}},-\eta_n)$, $\text{Rot1}(dF_z,-i)$ and $\text{Rot2}(dF_y,90-k_r)$ from Eqs. (4), (5), (6), (8), and (9) into Eq. (13), the elemental thrust dF_z, and the elemental radial forces dF_x and dF_y can be written in terms of the normal and friction forces acting on the element as:

$$|dF_z| = dF_f(\cos i \cos \gamma_n \sin k_r + \cos i \cos k_r \sin i - \cos i \cos k_r \sin i \sin \gamma_n) - dF_n(\cos k_r \cos \gamma_n \sin i + \sin k_r \sin \gamma_n) \quad (14)$$

$$|dF_x| = dF_f\{\sin^3 i + \cos^2 i[-\cos k_r \cos \gamma_n + \sin i(\sin k_r + \sin \gamma_n - \sin \gamma_n \sin k_r)]\} + dF_n \cos i(-\cos \gamma_n \sin i \sin k_r + \sin i \cos \gamma_n + \sin \gamma_n \cos k_r) \quad (15)$$

$$|dF_y| = dF_f \cos i[\cos k_r \cos \gamma_n \sin i + \cos^2 i \sin \gamma_n + \sin^2 i(1 - \sin k_r + \sin k_r \sin \gamma_n)] + dF_n[\cos \gamma_n(\cos^2 i + \sin^2 i \sin k_r) - \cos k_r \sin i \sin \gamma_n] \quad (16)$$

All the analysis above was based on the elemental cutting mechanism; consequently all the forces are referred to as elemental forces. At this point one can begin to investigate the resultant force that accounts for the action of the whole cutting edge.

3 Force System Acting on the Spade Bit

The so far formulated elemental cutting forces will be used in this section to define the cutting action of the whole cutting edge, i.e., of the forces that would correspond to the measured cutting forces. Because the spade drill bit, as shown in Fig. 2, has three characteristic cutting edges (chisel edge, tip cutting edge and major cutting edge), the resultant cutting force acting on the spade drill bit is the sum of the force components acting on each of these cutting edges, i.e.:

$$\begin{cases} F_z = F_z^{\text{chisel}} + F_z^{\text{tip}} + F_z^{\text{major}} \\ M_z = M_z^{\text{chisel}} + M_z^{\text{tip}} + M_z^{\text{major}} \end{cases} \quad (17)$$

The subsequent sub-sections will discuss in detail the constituent force components that act on the major cutting edge, tip cutting edge and chisel edge respectively, as expressed by Eq. (17).

3.1 Force Model for the Major Cutting Edge. In drilling operations the tangential cutting velocity is a linear function of the radial distance and increases outward from the drill's axis. Furthermore, it has been determined in [1,2] that the rake and inclination angles are also functions of the radial distance of the element from the drill's axis. Therefore, according to Eqs. (2) and (3), the specific normal and specific friction forces vary along the cutting edges of the drill-bit. Consequently, the model of the cutting edge forces should account for the variations of the normal rake angle and tangential cutting velocity, and must be able to predict the variations of the specific cutting pressure and of the forces along the cutting edges. As a consequence of these variations, Eq. (3) should be rewritten as:

$$K_n(r) = a_0 t_c^{a_1} V(r)^{a_2} e^{a_3 \gamma_n(r) + a_4 \alpha_n(r)}$$

$$K_f(r) = b_0 t_c^{b_1} V(r)^{b_2} e^{b_3 \gamma_n(r) + b_4 \alpha_n(r)} \quad (18)$$

where $V(r)$, $\alpha_n(r)$ and $\gamma_n(r)$ are expressing the dependence of the cutting velocity and of the clearance and rake angle on the radial distance of the element, r, from the drill's axis.

Since the specific cutting forces on the cutting edges are functions of the radial coordinate, the cutting forces at a given point can be computed by multiplying the specific cutting pressure by the elemental chip load at that point (Fig. 3). The chip area for a specific element is equal to $f_r/2\, dx$, where dx is the elemental length along the projection of the cutting edge on the plane normal to the drill axis and f_r is the chip-load expressed in [mm/rev]. From Eq. (1), the elemental specific normal and specific friction forces can be expressed as functions of the radial coordinate and rewritten as:

$$dx = \cos i(r)\, dr \quad (19)$$

$$dA_c = \frac{1}{2} dx f_r \sin k_r / \sin k_r = \frac{1}{2} f_r \cos i(r)\, dr \quad (20)$$

$$dF_n(r) = K_n(r) \frac{f_r}{2} \cos i(r)\, dr \quad (21)$$

$$dF_f(r) = K_f(r) \frac{f_r}{2} \cos i(r)\, dr \quad (22)$$

where $i(r)$ is the inclination angle at a specific point, and where $K_n(r)$ and $K_j(r)$ are respectively the normal specific force whose direction is normal to the rake face and the specific friction force which acts in the chip flow direction.

Now the resultant cutting forces for any part of a cutting edge of the drill-bit can be obtained by integrating between appropriate limits. The thrust force and torque equations for the major cutting edge can be written in terms of the integral of the elemental thrust force and torque as:

$$F_z^{\text{major}} = \int_{rp}^{R} 2\, dF_z(r) \quad (23)$$

$$M_z^{\text{major}} = \int_{rp}^{R} 2\, dM_z(r) \quad (24)$$

where rp is the radius of the tip cutting edge outer point and is equal to $w/2$ according to Fig. 2.

Since most drill-bits are symmetric, the cutting edge on each side generates its own radial forces, but the forces act in opposite directions, so the measured radial force represents their difference. The expressions for the radial forces presented below refer to one cutting edge, and can be written as:

$$F_x^{\text{major}} = \int_{rp}^{R} dF_x(r) \quad (25)$$

$$F_y^{\text{major}} = \int_{rp}^{R} dF_y(r) \quad (26)$$

where dF_x and dF_y were given by Eqs. (12) and (14). By substituting dM_z, dF_z, $dF_n(r)$ and $dF_f(r)$ from Eqs. (12), (14), (21) and (22) into Eqs. (23) and (24), the thrust force and torque can be written in terms of the normal and friction forces of the element. The resulting expressions are:

$$F_z^{\text{major}} = f_r \int_{rp}^{R} [K_f(r)\cos^2 i(r)(\cos \gamma_n(r)\sin k_r + \sin i(r)\cos k_r - \sin i(r)\cos k_r \sin \gamma_n(r)) - K_n(r)\cos i(r) \times (\sin i(r)\cos k_r \cos \gamma_n(r) + \sin k_r \sin \gamma_n(r))]\, dr \quad (27)$$

$$M_z^{\text{major}} = f_r \int_{rp}^{R} [K_f(r)[(\sin^2 i(r)\cos i(r) + \cos^3 i(r)\sin \gamma_n(r)] + K_n(r)\cos \gamma(r)_n \cos^2 i(r)]r\, dr \quad (28)$$

The radial forces acting on one cutting edge, in turn, are:

$$F_x^{\text{major}} = f_r \int_{rp}^{R} [K_f(r)\{\sin^3 i \cos i + \cos^3 i[-\cos k_r \cos \gamma_n + \sin i(\sin k_r + \sin \gamma_n - \sin \gamma_n \sin k_r)]\} + K_n(r)\cos^2 i(-\cos \gamma_n \sin i \sin k_r + \sin i \cos \gamma_n + \sin \gamma_n \cos k_r)]\, dr \quad (29)$$

$$F_y^{\text{major}} = f_r \int_{rp}^{R} \{K_f(r)\cos^2 i[\cos k_r \cos \gamma_n \sin i + \cos^2 i \sin \gamma_n + \sin^2 i(1-\sin k_r + \sin k_r \sin \gamma_n)] + K_n(r)\cos i[\cos \gamma_n(\cos^2 i + \sin^2 i \sin k_r) - \cos k_r \sin i \sin \gamma_n]\} dr \quad (30)$$

For numerical prediction purposes and prediction software development the above results can be expressed in discrete form by substituting the integration by summation. Then, the corresponding numerical expressions for the discrete resultant force model for the major cutting edge is obtained as the sum of all elemental forces that are involved in cutting, i.e.:

$$\begin{cases} F_z^{\text{major}} = \sum_{n=1}^{N_m} dF_z(n) \\ M_z^{\text{major}} = \sum_{n=1}^{N_m} dM_z(n) \end{cases} \quad (31)$$

where N_m is the number of elements of the major cutting edge. $dF_z(n)$ and $dM_z(n)$ correspond to the nth element's elemental thrust force and torque respectively. According to Eqs. (14) and (12), the corresponding numerical expressions for the elemental forces are:

$$\begin{cases} dF_z(n) = 0.5 f_r \{K_f(n)\cos^2 i(n)[\cos \gamma_n(n)\sin k_r + \sin i(n)\cos k_r(1-\sin \gamma_n(n))] \\ \quad - K_n(n)\cos i(n)[\sin i(n)\cos k_r \cos \gamma_n(n) + \sin k_r \sin \gamma_n(n)]\} \Delta r \\ \qquad\qquad\qquad\qquad\qquad\qquad\qquad\qquad\qquad\qquad n = 1,2,\ldots N_m \\ dM_z(n) = 0.5 f_r r(n)\{K_f(n)[\sin^2 i(n)\cos i(n) + \cos^3 i(n)\sin \gamma_n(n)] \\ \quad + K_n(n)\cos^2 i(n)\cos \gamma_n(n)\} \Delta r \end{cases} \quad (32)$$

here

$$\begin{cases} K_n(n) = a_0 \left(\frac{f_r}{2}\right)^{a_1} [\Omega r(n)]^{a_2} e^{a_3 \gamma_n(n) + a_4 \alpha_n(n)} \\ K_f(n) = b_0 \left(\frac{f_r}{2}\right)^{b_1} [\Omega r(n)]^{b_2} e^{b_3 \gamma_n(n) + b_4 \alpha_n(n)} \end{cases} \quad (33)$$

and Ω is the spindle speed, Δr is the radial length of the cutting element, $r(n)$ is the distance between the Z-axis to the nth cutting element, $\alpha_n(n)$ is the clearance angle of the nth cutting element, and $\gamma_n(n)$ is the rake angle of the nth cutting element.

3.2 Force Model for the Tip Cutting Edge. In analogy to the derivations for the major cutting edge, the corresponding force model for the tip cutting edge can be determined by following the same procedure. By replacing the major cutting edge point angle k_r with the tip point angle ρ, the tip cutting edge thrust force and torque can be written in terms of the normal and friction forces of the element as:

$$F_z^{\text{tip}} = f_r \int_{rc}^{rp} [K_f(r)\cos^2 i(r)(\cos \gamma_n(r)\sin(\rho) + \sin i(r)\cos(\rho) - \sin i(r)\cos(\rho)\sin \gamma_n(r)) - K_n(r)\cos i(r) \times (\sin i(r)\cos(\rho)\cos \gamma_n(r) + \sin(\rho)\sin \gamma_n(r))] dr \quad (34)$$

$$M_z^{\text{tip}} = f_r \int_{rc}^{rp} [K_f(r)[(\sin^2 i(r)\cos i(r) + \cos^3 i(r)\sin \gamma_n(r)] + K_n(r)\cos \gamma(r)_n \cos^2 i(r)] r dr \quad (35)$$

The radial forces acting on one tip cutting edge are:

$$F_x^{\text{tip}} = f_r \int_{rc}^{rp} [K_f(r)\{\sin^3 i \cos i + \cos^3 i[-\cos(\rho)\cos \gamma_n + \sin i(\sin(\rho) + \sin \gamma_n - \sin \gamma_n \sin(\rho))]\} + K_n(r)\cos^2 i(-\cos \gamma_n \sin i \sin(\rho) + \sin i \cos \gamma_n + \sin \gamma_n \cos(\rho))] dr \quad (36)$$

$$F_y^{\text{tip}} = f_r \int_{rc}^{rp} \{K_f(r)\cos^2 i[\cos(\rho)\cos \gamma_n \sin i + \cos^2 i \sin \gamma_n + \sin^2 i(1-\sin(\rho) + \sin(\rho)\sin \gamma_n)] + K_n(r)\cos i[\cos \gamma_n(\cos^2 i + \sin^2 i \sin(\rho)) - \cos(\rho)\sin i \sin \gamma_n]\} dr \quad (37)$$

here rc is the radial distance between the chisel edge outer point and drill bit axis Z, and rp is the radial distance between the tip cutting edge outer point and drill bit axis Z.

Similarly, the corresponding discrete model for the tip cutting edge can be written as:

$$\begin{cases} F_z^{\text{tip}} = \sum_{n=1}^{N_t} dF_z(n) \\ M_z^{\text{tip}} = \sum_{n=1}^{N_t} dM_z(n) \end{cases} \quad (38)$$

where N_t is the number of elements engaged in cutting at that cutting moment. This number changes with the spade bit's penetration into the workpiece. $dF_z(n)$ and $dM_z(n)$ are the elemental thrust force and torque for nth element, i.e.:

$$\begin{cases} dF_z(n) = 0.5 f_r \{K_f(n)\cos^2 i(n)[\cos \gamma_n(n)\sin \rho + \sin i(n)\cos \rho(1-\sin \gamma_n(n))] \\ \quad - K_n(n)\cos i(n)[\sin i(n)\cos \rho \cos \gamma_n(n) + \sin \rho \sin \gamma_n(n)]\} \Delta r \\ \qquad\qquad\qquad\qquad\qquad\qquad\qquad\qquad\qquad\qquad n = 1,2,\ldots N_t \\ dM_z(n) = 0.5 f_r r(n)\{K_f(n)[\sin^2 i(n)\cos i(n) + \cos^3 i(n)\sin \gamma_n(n)] \\ \quad + K_n(n)\cos^2 i(n)\cos \gamma_n(n)\} \Delta r \end{cases} \quad (39)$$

3.3 Force Model for the Chisel Edge. Oxford [19] has shown that for drilling, in a small region around the center of the chisel edge, the tool does not actually cut but instead extrudes the material. This region is called the indentation zone. The portion of the chisel edge outside the indentation zone is referred to as the secondary cutting edge. It is accepted practice to determine the forces at the secondary cutting edges by using the same type of mechanistic models as for the major cutting edges [6,7].

Due to the simple profile of the chisel edge for spade bits, the chisel edge cutting process is a normal cutting process, with no inclination angle and with a 90° cutting edge point angle. So, in terms of the normal and friction forces acting on the elements, the chisel edge thrust force and torque can be written as:

$$F_z^{\text{chisel}} = f_r \int_0^{rc} [K_f(r)\cos\gamma_n(r) - K_n(r)\sin\gamma_n(r)]dr \quad (40)$$

$$M_z^{\text{chisel}} = f_r \int_0^{rc} [K_f(r)\sin\gamma_n(r) + K_n(r)\cos\gamma_n(r)]r\,dr \quad (41)$$

The radial forces acting on one chisel cutting edge are:

$$F_x^{\text{chisel}} = f_r \int_0^{rc} [-K_f(r)\cos\gamma_n(r) + K_n(r)\sin\gamma_n(r)]dr \quad (42)$$

$$F_y^{\text{chisel}} = f_r \int_0^{rc} [K_f(r)\sin\gamma_n(r) + K_n(r)\cos\gamma_n(r)]dr \quad (43)$$

and the corresponding discrete numerical models are:

$$\begin{cases} F_z^{\text{chisel}} = \sum_{n=1}^{N_c} dF_z(n) \\ M_z^{\text{chisel}} = \sum_{n=1}^{N_c} dM_z(n) \end{cases} \quad (44)$$

where N_c is the total number of elements of the chisel edge and $dF_z(n)$ and $dM_z(n)$ are the elemental thrust force and torque given by:

$$\begin{cases} dF_z(n) = 0.5 f_r (K_f(n)\cos\gamma_n(n) - K_n(n)\sin\gamma_n(n))\Delta r \\ dM_z(n) = 0.5 f_r r(n)(K_f(n)\sin\gamma_n(n) + K_n(i)\cos\gamma_n(n))\Delta r \end{cases} \quad n = 1,2,\ldots N_c \quad (45)$$

The above expressions, for the sake of simplicity, neglect the indentation effects, consider the nominal values of the cutting velocity without considering the influence of the feed velocity and are based on the static instead of the dynamic values of the rake and clearance angles. This assumption is justifiable because the influence of the chisel edge, in comparison to the tip and major cutting edges, is generally small for spade drills.

3.4 Model of the Resultant Force. The derivations in the last three sub-sections facilitate the complete evaluation of the resultant forces acting on the spade bit given by Eq. (17) by substituting the appropriate expressions for the characteristic cutting edges in accordance to Eqs. (27, 28, 34, 35, 40 and 41). It is clear that the elemental specific normal force $K_n(r)$ and friction force $K_f(r)$ are functions of the arbitrary cutting element's cutting angles and cutting velocity. The general resultant forces and torque are based on the individual cutting element, and as such the force and torque models exploit the inherent variation of the cutting angles and of the tangential cutting velocity along the cutting edges of the spade bit. Consequently this force model suits any kind of spade point geometry, including the straight flat spade bit or curved spade bits [2]. The following section will focus on the calibration of the model, that is, the determination of the unknown coefficients in Eq. (18) of the specific force model.

4 Coefficient Calibration

The drill point geometry and the mechanistic force models have facilitated the establishment of the relationship between the spade drill bits' geometry and the cutting force system acting on its principal edges. However, the underlying relationships were based on the assumption that the coefficients of the mechanistic force model were known. In this section, a calibration procedure and algorithm to obtain the applicable oblique-cutting model coefficients from experimental drilling thrust and torque data will be developed.

Tests that are easy to perform in an industrial environment are desirable for model calibration. To accomplish this goal it will be shown that the developed model can be calibrated based on a suitable set of experiments that are performed using a set of tools (with different normal rake angles and normal clearance angles) and different combinations of cutting conditions.

4.1 Theoretical Background for a Simplified Calibration Procedure. The purpose of the calibration procedure is to find the force model coefficients from experimental data. From the mechanistic force model expressions (Eqs. (27), (28), (34), (35), (40), and (41)) of the spade drill bit, it can be seen that the force expressions are too complex for calibrating the coefficients. Consequently, in the sequel a special experimental configuration will be introduced and simplified approximate expressions for the specific normal and friction force will be formulated.

To simplify the calibration procedure a straight-flat spade bit with a cutting edge point angle k_r equal to 90 deg will be assumed in a drilling operation with a pilot hole to eliminate the cutting actions of the spade bit's tip cutting edge and chisel edge as shown in Fig. 6.

For the assumed configuration, the drill bit's drilling thrust force and torque during cutting can be rewritten, based on Eqs. (27) and (28), as:

$$F_z = f_r \int_{rh}^{R} [K_f(r)\cos^2 i(r)\cos\gamma_n(r) - K_n(r)\cos i(r)\sin\gamma_n(r)]dr \quad (46)$$

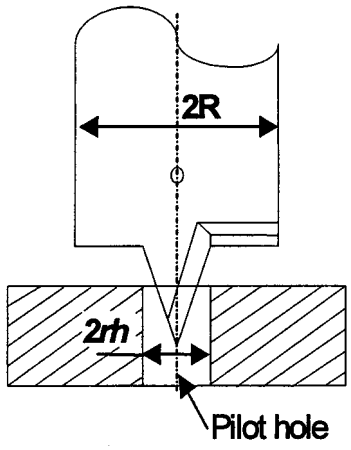

Fig. 6 Experiment with pilot hole

$$M_z = f_r \int_{rh}^{R} [K_f(r)[(\sin^2 i(r)\cos i(r) + \cos^3 i(r)\sin \gamma_n(r)] + K_n(r)\cos \gamma_n(r)\cos^2 i(r)]rdr \quad (47)$$

where rh is the radius of the pilot hole and R is the radius of the drill bit.

The cutting velocity V at an arbitrary point of the cutting edge is equal to the product of Ω, the spindle speed and r, the radial distance of the cutting point from the drill axis, implying that it changes with radial distance. Also, the rake and clearance angles change with radial distance. Hence, the specific normal and friction forces (Eq. (18)) are a function of the radial distance. In light of this and in order to further simplify the calibration procedure two additional assumptions will be made: (1) the average cutting velocity will be used to represent the changing cutting velocity for each of the major cutting edge elements and (2) the rake and clearance angle distribution along the major cutting edge will be assumed constant by substituting the average rake and clearance angle values γ_n and α_n for $\gamma_n(r)$ and $\alpha_n(r)$.

The rationale for the adoption of the above assumptions is the formulation of a simple calibration procedure. Since the suggested procedure calls for the use of a pilot hole with diameter rh whose value is generally a substantial portion of the drill radius R the adoption of the average instead of the actual velocity for each of the cutting edge elements engaged in cutting on the outcome is not expected to be significant. On the other hand, the detailed analysis of the cutting angle distributions along the major cutting edge given by Zhao [1] and Zhao et al. [2] for different spade drill topologies provides a conclusive argument in favor of using the average instead of actual values of the rake and clearance angles of the respective elements since they do not change significantly for the portion of the major cutting edge engaged with the workpiece during the proposed calibration procedure. If one desires to minimize the influence of the variable nature of the relevant variables the pilot hole radius can be increased. Comprehensive validation experiments, to be presented later, will confirm the minimal influence of these assumptions on the prediction accuracy of the models. Under the preceding simplifying assumptions the specific normal and specific friction forces at any arbitrary cutting point along the major cutting edge can be rewritten as:

$$K_n = a_0 t_c^{a_1} \left(\frac{rh+R}{2} \right)^{a_2} \Omega^{a_2} e^{a_3\gamma_n + a_4\alpha_n} \quad (48)$$

$$K_f = b_0 t_c^{b_1} \left(\frac{rh+R}{2} \right)^{b_2} \Omega^{b_2} e^{b_3\gamma_n + b_4\alpha_n} \quad (49)$$

Alternatively, the use of the last two expressions can be viewed as the replacement of the variable specific forces by their constant counterparts that correspond to the average cutting conditions at the major cutting edge.

Substituting Eqs. (48) and (49) into Eqs. (46) and (47), the drilling thrust force and torque can be expressed as:

$$F_z = f_r \int_{rh}^{R} [K_f \cos \gamma_n \cos^2 i(r) - K_n \sin \gamma_n \cos i(r)]dr \quad (50)$$

$$M_z = f_r \int_{rh}^{R} [K_f(\cos^3 i(r)\sin \gamma_n + \sin^2 i(r)\cos i(r) + K_n \cos \gamma_n \cos^2 i(r)]dr \quad (51)$$

A general expression for the inclination angle, i, as a function of the normalized radial distance r, is given elsewhere (e.g., [1,2]). Here however, since it was assumed that $k_r = 90$ deg, the general expression for the inclination angle can be simplified and written as:

$$i(r) = \sin^{-1}\left(\frac{t}{2r} \right) \quad (52)$$

Based on Eq. (52) $\cos i(r)$, that appears in Eqs. (50) and (51), can be written as:

$$\cos i(r) = \{1 - \sin^2 i(r)\}^{1/2} = \sqrt{1 - \frac{t^2}{4r^2}} \quad (53)$$

The Taylor series expansion of the last equation yields the following approximate expression for $\cos i(r)$:

$$\cos i(r) \cong 1 - \frac{1}{8}\frac{t^2}{r^2} - \frac{1}{128}\frac{t^4}{r^4} \quad (54)$$

Now by substituting the values of $i(r)$ and $\cos i(r)$ given by Eqs. (52) and (54) into Eqs. (50) and (51), and performing the necessary integration, the thrust force and torque can be written as:

$$F_z = f_r K_f \cos \gamma_n (r + t^2/8)\Big|_{rh}^{R} - f_r K_n \sin \gamma_n (r + t^2/8 + t^4/(384r^3))\Big|_{rp}^{R} \quad (55)$$

$$M_z = f_r K_f \left[\frac{t^2}{8}\sin \gamma_n + 0.25(1 - 1.5\sin \gamma_n)t^2 \ln r + \frac{t^4}{32r^2}\left(0.5 - \frac{3}{8}\sin \gamma_n \right) + \frac{t^6}{2048r^4}(1 - \sin \gamma_n) \right]\Bigg|_{rh}^{R} + f_r K_n \cos \gamma_n \left(\frac{1}{2}r^2 - W^2 \ln r \right)\Bigg|_{rh}^{R} \quad (56)$$

The solution of Eqs. (55) and (56), yields the specific normal and friction forces in the form:

$$K_f = \frac{F_z T_n + M_z R_n}{f_r(R_f T_n + R_n T_f)} \quad (57)$$

$$K_n = \frac{-F_z T_f + M_z R_f}{f_r(R_f T_n + R_n T_f)} \quad (58)$$

where

$$R_f = \cos \gamma_n (r + t^2/2)\Big|_{rh}^{R} \quad (59)$$

$$R_n = \sin \gamma_n (r + t^2/8 + t^4/(384r^3))\Big|_{rh}^{R} \quad (60)$$

$$T_f = \frac{r^2}{2}\sin \gamma_n + 0.25(1 - 1.5\sin \gamma_n)t^2 \ln r + \frac{t^4}{32r^2}\left(0.5 - \frac{3}{8}\sin \gamma_n \right) + \frac{t^6}{2048r^4}(1 - \sin \gamma_n)\Big|_{rh}^{R} \quad (61)$$

$$T_n = \cos \gamma_n \left(\frac{1}{8}t^2 - \frac{1}{4}t^2 \ln r \right)\Bigg|_{rh}^{R} \quad (62)$$

It is evident from Eqs. (57) and (58), that the specific normal and friction forces can be obtained if experimental measurements, performed in accordance to the configuration shown in Fig. 6, of the appropriate force and torque components are available.

When a drill bit with $k_r = 90$ deg is not available, the same procedure is still valid. The only difference is that coefficients R_f and R_n in Eqs. (57) and (58) should account for the particular value of k_r. These more general expressions are given by:

$$R_f = \sin k_r \cos \gamma_n (r + t^2/8) + 0.5(1 - \sin \gamma_n)\cos k_r t \ln r\Big|_{rh}^{R} \quad (63)$$

$$R_n = \sin k_r \sin \gamma_n (r + t^2/(8r) + t^4/(384r^3)) + \cos k_r \cos \gamma_n (0.5t \ln r + t^3/(32r^2) + t^5/(1024r^4))\Big|_{rp}^{R} \quad (64)$$

The proposed calibration procedure can be therefore performed by different types of major cutting edge configurations.

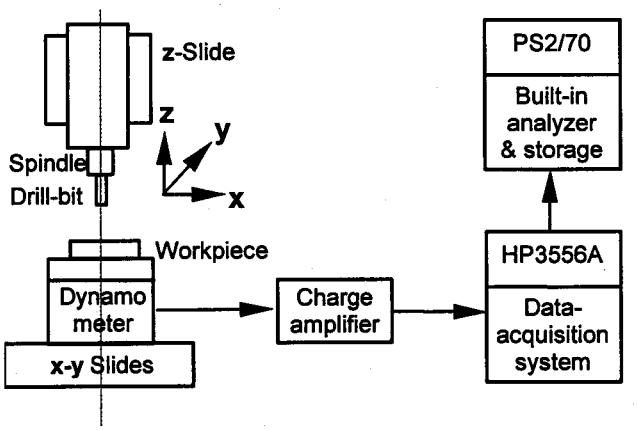

Fig. 7 Block diagram of the experimental setup

4.2 Experimental Procedure and Coefficient Estimation The experimental configuration corresponds to that shown in Fig. 6 in which the three orthogonal force components and torque are measured. The average values of the force and torque are used in the calibration expressions.

The experiments were performed on a Cincinnati Milacron Saber 750 Vertical Machining Center that was instrumented to allow the measurement of drilling torque, thrust and radial force components. The block diagram of the experimental setup is shown in Fig. 7. Force and torque measurements were performed by a four-component KISTLER piezo-electric drilling dynamometer. The specimens were mounted on a vise attached to the dynamometer's platform resulting, due to the small weight of the vise and specimen, in the retention of the wide frequency band of the dynamometer's response (approximately 3 kHz). The signals were amplified by charge amplifiers and digitized by a HP multi-channel data acquisition system. The drills were held in the spindle by a standard 1/4 in. collet to minimize drill shank run-out effects as much as possible.

Since all the acquired drilling thrust and torque signals have exhibited a very strong dynamic variation component with a frequency equal to the rotational frequency of the drill, the thrust and torque signals were digitally filtered by a fourth order Butterworth digital filter during data analysis to remove the dynamic component of the signal, mainly caused by runout and vibrations, to make the assessment of the average thrust and torque values easier. The filter cutoff frequencies were set lower than the drill's rotational frequency at 5 Hz. The data were filtered and analyzed using *MATLAB*.

The workpiece material used was medium density fiberboard (MDF). This material was used because of its isotropic and constant mechanical properties, unlike natural wood, which makes comparisons much easier and meaningful. The actual cutting conditions will be stated for each set of experiments reported in the sequel. The same procedure would be applicable for wood as well. In this case, however, the obtained coefficients would represent an average value due to the anisotropic nature of wood.

A minimal plausible experimental design matrix for coefficient calibration could, for example, utilize four spade bits with two different rake and two different clearance angles used at two cutting speed and feed levels. This would result in a minimum of 16 experiments. For more accurate calibration, however, some of the experiments may be repeated or the experimental matrix expanded. The desired range of the validity of the calibrated model will dictate the specific range of the geometric and operational parameters.

The estimation of the calibration constants in Eqs. (48) and (49) requires, as the first step, the evaluation of the specific normal force K_n and of the specific friction force K_f utilizing the measured torque and thrust force values in accordance with Eqs. (57) and (58). Subsequently, a suitable non-linear parameter estimation procedure can be used to evaluate the calibration constants in Eqs. (48) and (49) with the computed specific normal force K_n and of the specific friction force K_f as the dependent variables. In the current work the "NonLinearFit" function from the *MATHEMATICA* software package was used to obtain the coefficients.

The above procedure was implemented to derive the calibration coefficients in accordance with Eqs. (57) and (58) for a particular set of cutting conditions. Experiments were performed with a pilot hole using nine tools characterized by different major cutting edge geometries, i.e., three rake angles (10, 14 and 18 degrees) and three clearance angles (10, 12 and 14 degrees) under the following cutting conditions: 400 and 800 rpm spindle speed and 190, 381 and 762 mm/min feedrate. The use of the measured values in Equations (48) and (49) in conjunction with the "NonLinearFit" routine yielded the following expressions for the specific normal and friction forces as a function of cutting conditions:

$$K_n = e^{6.879} t_c^{-0.065} V^{0.0566} e^{-1.943\gamma + 0.0606\alpha} \tag{65}$$

$$K_f = e^{4.209} t_c^{-0.558} V^{0.0414} e^{-0.3155\gamma + 0.3155\alpha} \tag{66}$$

To verify the accuracy of the calibration coefficients, they were substituted into Eq. (31), along with the appropriate machining conditions and tool geometry for a different set of drills and conditions from those used in the calibration process. Experiments were again performed with nine different major cutting edge geometries, i.e., rake angles of 10, 14 and 18 degrees and clearance angles of 8, 11 and 14 degrees with cutting speeds of 400 and 800 rpm and feedrates of 127, 254 and 508 mm/min. These experiments were replicated twice (detailed data are given in [1]) while a typical complete process simulation is also shown in Fig. 1 of Part 2). The measured and calculated values of the thrust and torque for these conditions have yielded average torque and thrust force prediction errors of 3.08% and 8.74% respectively. It is apparent that the accuracy of the torque predictions is higher than that for the thrust. In the latter case, prediction accuracy has deteriorated with an increase in the magnitude of the rake angle.

In Part 2 of this paper the specific cutting force coefficients given by Eqs. (63) and (64) will be used in all simulation examples. These coefficients were assumed to be valid for the cutting actions of the major cutting edge, tip cutting edge and the secondary cutting edge portion of the chisel edge.

5 Conclusions

The main points resulting from the content presented above are:

1. Chip removal related force models were formulated for general spade bit topologies.
2. A cutting elemental mechanistic model was introduced.
3. The relationships between force components in different coordinate frames were derived.
4. Force models, which account for the influence of drill geometry and machining conditions, were given.
5. A coefficient calibration method was introduced that was based on a simplified formulation of the expressions for the cutting coefficients and on a simple experimental procedure.

The developed model includes the cutting action of all characteristic edges of the spade bit and is, as a consequence of this, able to predict the complete force system in spade drilling operations throughout all phases of the process (from entry to exit).

Acknowledgments

The support of American Tool Inc., of NSF under grant #DMI 98-13457 and of the NSF/DARPA funded Machine Tool Agile Manufacturing Research Institute (MTAMRI) is gratefully acknowledged.

References

[1] Zhao, H., 2000, ''Geometry and Mechanics of Spade Drilling Operations,'' Ph.D. Thesis, Northwestern University, Evanston, Illinois.

[2] Zhao, H., and Ehmann, K. F., 2001 (Under review), ''Topology of Spade Drills for Wood Drilling Operations-Part 1: Spade Drill Point Geometry Definition and Part 2: Spade Drill Point Cutting Geometry Analysis,'' ASME J. Manuf. Sci. Eng. .

[3] Kline, W. A., DeVor, R. E., and Lindberg, J. R., 1982, ''The Prediction of Cutting Force in End Milling with Application to Cornering Cuts,'' Int. J. Mach. Tool Des. Res., **22**(1), pp. 7–22.

[4] Yucesan, G., and Altintas, Y., 1993, ''Mechanics of the Ball End Milling Process,'' ASME Winter Annual Meeting, PED-64, pp. 543–552.

[5] Williams, R. A., 1974, ''A Study of the Drilling Process,'' ASME J. Eng. Ind., **106**(4), pp. 1207–1215.

[6] Watson, A. R., 1985, ''Drilling Model for Cutting Lip and Chisel Edge and Comparison of Experimental and Predicted Results. I—Initial Cutting Lip Model, II—Revised Cutting Lip Model, III—Drilling Model for Chisel Edge and IV—Drilling Tests to Determine Chisel Edge Contribution to Torque and Thrust,'' Int. J. Mach. Tool Des. Res., **25**(4), pp. 347–406.

[7] Watson, A. R., 1985, ''Geometry of Drill Elements,'' Int. J. Mach. Tool Des. Res., **25**(3), pp. 209–227.

[8] Chandrasekharan, V., Kapoor, S. G., and DeVor, R. E., 1995, ''A Mechanistic Approach to Predicting the Cutting Forces in Drilling: With Application to Fiber-Reinforced Composite Materials,'' ASME J. Eng. Ind., **117**(4) pp. 559–570.

[9] Chandrasekharan, V., Kapoor, S. G., and DeVor, R. E., 1997, ''A Calibration Procedure for Fundamental Oblique-Cutting Model Coefficients Based on A Three-Dimensional Mechanistic Drilling Force Model,'' Transactions of NAMRI/SME, **XXV**, pp. 255–260.

[10] Budak, E., and Altintas, Y., 1993, ''Prediction of Milling Force Coefficients from Orthogonal Cutting Data,'' ASME Winter Annual Meeting, PED-64, pp. 453–460.

[11] Shin, Y. C., and Waters, A. J., 1997, ''A New Procedure to Determine Instantaneous Cutting Force Coefficients for Machining Force Prediction,'' Int. J. Mach. Tools Manuf., **37**(9), pp. 1337–1351.

[12] Stephenson, D. A., and Agapiou, J. S., 1992, ''Calculation of Main Cutting Edge Forces and Torque for Drills with Arbitrary Point Geometries,'' Int. J. Mach. Tools Manuf. **32**(4), pp. 521–538.

[13] Armarego, E. J. A., and Cheng, C. Y., 1972, ''Drilling With Flat Rake Face and Conventional Twist Drill-I. Theoretical Investigation,'' Int. J. Mach. Tool Des. Res., **12**, pp. 17–35.

[14] Armarego, E. J. A., and Wright, J. D., 1984, ''Predictive Models for Drilling Thrust and Torque-A Comparison of Three Flank Configurations,'' CIRP Ann., **33**(1), p. 5.

[15] Merchant, M. E., 1945, ''Basic Mechanics of the Metal-Cutting Process,'' ASME J. Appl. Mech., **66** A-168–A-175.

[16] Gu, F., Kapoor, S. G., DeVor, R. E., and Bandyopadhyay, P., 1992, ''A Cutting Force for Face Milling with a Step Cutter,'' Transactions of NAMRI/SME, **XX**, pp. 361–367.

[17] Endres, W. J., and Waldorf, D. J., 1994, ''The Importance of Considering Size Effect Along the Cutting Edge in Predicting the Effective Lead Angle for Turning,'' Transactions of NAMRI/SME, **XXII**, pp. 65–72.

[18] Stabler, G. V., 1964, ''The Chip Flow Law and its Consequences,'' *Advances in Machine Tool Design and Research*, Oxford: Pergamon Press, Ltd., p. 243.

[19] Oxford, C. J., 1955, ''On the Drilling of Metals I-Basic Mechancis of the Process,'' Trans. ASME, **77**, pp. 103–114.